Coordination-Directed Self-Assembly of $M_{12}L_{24}$ Nanocage: Effects of Kinetic Trapping on the Assembly Process

Makoto Yoneya,[†,*] Seiji Tsuzuki,[†] Tomohiko Yamaguchi,[†] Sota Sato,[‡,§] and Makoto Fujita[‡]

[†]Nanosystem Research Institute, National Institute of Advanced Industrial Science and Technology, 1-1-1 Umezono, Tsukuba 305-8568, Japan, and [‡]Department of Applied Chemistry, School of Engineering, University of Tokyo, 7-3-1 Hongo, Bunkyo-ku, Tokyo 111-8656, Japan. [§]Present address: Tohoku University, Sendai, Japan.

ABSTRACT We demonstrate the spontaneous formation of spherical complex $M_{12}L_{24}$, which is composed of 12 palladium ions and 24 bidentate ligands, by molecular dynamics simulations. In contrast to our previous study on the smaller M_6L_8 cage, we found that the larger $M_{12}L_{24}$ self-assembly process involves noticeable kinetic trapping at lower nuclearity complexes, *e.g.*, M_6L_{12}, M_8L_{16}, and M_9L_{18}. We also found that the kinetic trapping behaviors sensitively depend on the bend angle of ligands and the metal–ligand binding strength. Our results show that these kinetic effects, that have generally been neglected, are important factor in self-assembly structure determination of larger complexes as $M_{12}L_{24}$ in this study.

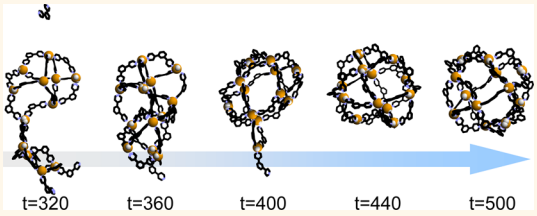

KEYWORDS: self-assembly · nanocage · metal–ligand coordination · kinetic trapping · molecular dynamics simulation

Coordination cages that are formed by the complexation of transition-metal ions with exomultidentate ligands have received much interest over the past decade.[1,2] For example, *n* metal ions (M) and *2n* pyridine-capped ligands (L) are reported to self-assemble into coordinated nanocages M_nL_{2n} for n = 2,[3,4] 6,[5] 12[6−8] and 24[9] in polar solvents. These nanocages can be used as molecular shells with various functions.[10−12] Understanding the mechanism underlying this supramolecular self-assembly is important for designing such functional nanocage materials. Computational studies can play a significant role in those research.[2]

In our previous study,[13] we proposed a simulation model for the self-assembly of the simplest spherical complex M_6L_8, which was composed of six palladium (Pd) ions and eight tridentate ligands.[14] In the real reaction system, the M_6L_8 complex can be readily formed from a 4:3 mixture of the tridentate ligand and $Pd(NO_3)_2$ in dimethyl sulfoxide (DMSO) solvent with a reaction time scale of minutes.[14] This time scale is far greater than the accessible time scale in common molecular dynamics (MD) simulations and we need to speed it up to fill the gap between the real reaction systems. Due to this general difficulty in atomistic (supra)molecular self-assembly simulation, only a few attempts have been reported that go further as to rationalize the principles of chemical design.[15] By applying the coarse-grained solvent model,[13] we succeeded in observing a spontaneous formation of the spherical shaped M_6L_8 cages over the course of the simulations, which were started from random initial placement of the metals and ligands. We found that the large difference in the lifetimes of the smaller incompleted clusters and the larger completed M_6L_8 nanocages is crucially important for self-assembly.

In this study, we applied our previous model to the larger spherical complex $M_{12}L_{24}$, which is a nanocage with 12 Pd(II) ions and 24 pyridine-capped bidentate ligands[8,16] shown in Figure 1, for example. $M_{12}L_{24}$ cages are most extensively studied among M_nL_{2n} cages[12] and proved to be used as functional molecular cages for the encapsulation of perfluoroalkanes,[17] the polymerization of methyl methacrylate segments[18] and the protection of a small protein.[19] Therefore, we think the development of simulation models for such $M_{12}L_{24}$ nanocages is important and valuable.

* Address correspondence to makoto-yoneya@aist.go.jp.

Received for review September 2, 2013 and accepted January 29, 2014.

Published online January 29, 2014
10.1021/nn404595j

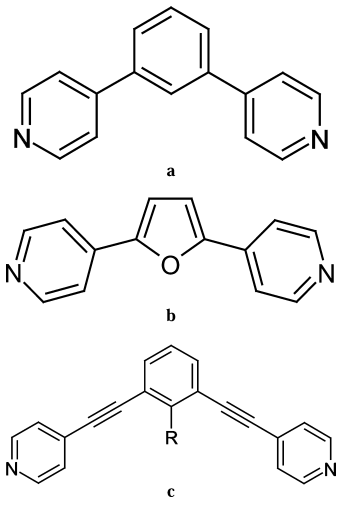

Figure 1. Pyridine-capped banana-shaped bidentate ligands a, b and c (R = OCH_3).

RESULTS AND DISCUSSION

To compare with the previous M_6L_8 case with the same solvent condition, we first used a relatively small system with an initial structure generated by random placement of 48 Pd(II) and 96 ligand **a** models (which corresponds to four $M_{12}L^a_{24}$ nanocages) without the explicit atomistic solvent.[13] The initial structure is shown in Figure 2a. The concentrations of the Pd(II) ions and ligands in the cubic simulation box (volume = 30 nm^3) were chosen to be comparable to the M_6L_8 system in our previous study.

Snapshots after the 500 ns Langevin dynamics (LD)[20] runs at the simulation temperature of 343 K (70 °C, the experimental reaction condition[8]) are shown in Figure 2b. As shown in the enlarged image in Figure 3, a complete $M_{12}L^a_{24}$ nanocage was successfully formed during this LD run. For all 12 Pd(II) within this completed nanocage in Figure 3, time variations of the coordination numbers (judged from the distance between Pd and ligand-nitrogen atoms with the specified threshold[13]) of each Pd(II) are shown in Figure 4. The time evolutions in this figure can be divided into three stages, an assembly stage up to *ca.* 100 ns, an evolution stage between 100 and 500 ns and a fixation stage above 500 ns. Structure change during the evolution stage is shown in Figure 5. The simulated three-stage process in Figure 4 corresponds well to the stages found in our previous simulations on the M_6L_8 system and that explained in the experimental study on $M_{12}L_{24}$ system.[21]

We also tried completely parallel simulations for the furan-cored ligand **b** shown in Figure 1. With this ligand **b**, we also observed the spontaneous formation of $M_{12}L^b_{24}$ nanocage as shown in Figure 6. From the results described above, we are convinced that our model, which was originally developed for the M_6L_8 system, is capable of demonstrating the self-assembly of the larger $M_{12}L_{24}$ system for two kinds of ligands shown in Figure 1.

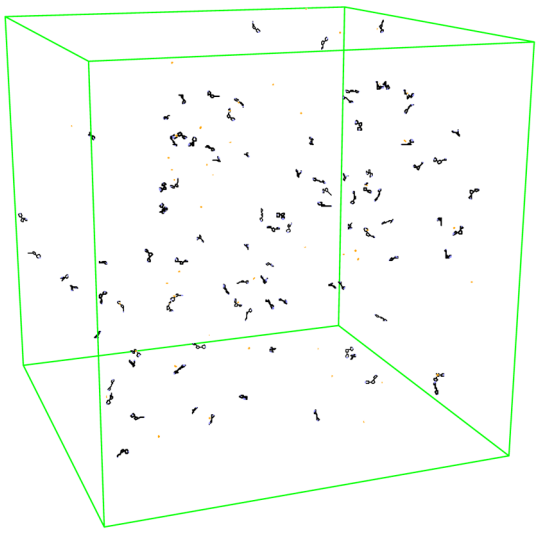

(a)

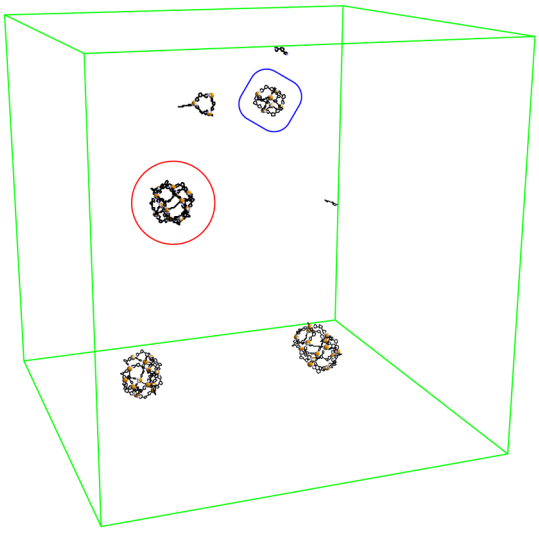

(b)

Figure 2. (a) Initial structure generated by random placement of 48 Pd(II) and 96 ligand a models in the cubic simulation box (volume = 30 nm^3). (b) Snapshot after a 500 ns LD run with $M_{12}L^a_{24}$ and $M_6L^a_{12}$ nanocages in the circle and square, respectively.

Next, we enlarged the system size to see the cluster size distribution evolution during the $M_{12}L_{24}$ nanocage formation. We constructed a system eight times larger than the first system (with 384 Pd(II) ions and 768 ligand **a** models which corresponds to 32 $M_{12}L^a_{24}$ nanocages) by doubly stacking the MD cells in each *XYZ* direction. As in our previous study,[13] we also incorporated 192 explicit solvent atoms of the CH united atom type into the above system. This solvent atom number (half of the Pd ion number) was the optimum number to speed up M_6L_8 cage formation in the previous study. A random initial structure was constructed through a 50 ns high-temperature (473 K) LD run using

uncharged Pd(II) models. The LD run with the original Pd(II) model was then performed for 1 μs at 343 K. The cluster size distributions were analyzed based on the ligand−metal coordination bonds from the simulated trajectories.

Figure 7 shows the ligand cluster size distributions as a function of time; the vertical axis corresponds to the

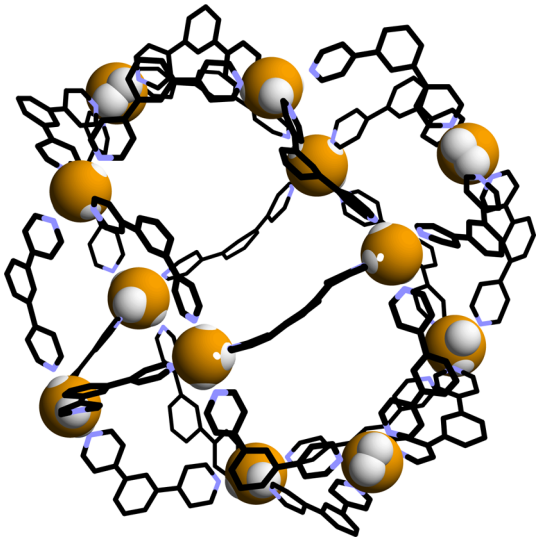

Figure 3. Enlarged view of the $M_{12}L_{24}^{a}$ nanocage from the snapshot after the 500 ns LD run in Figure 2b.

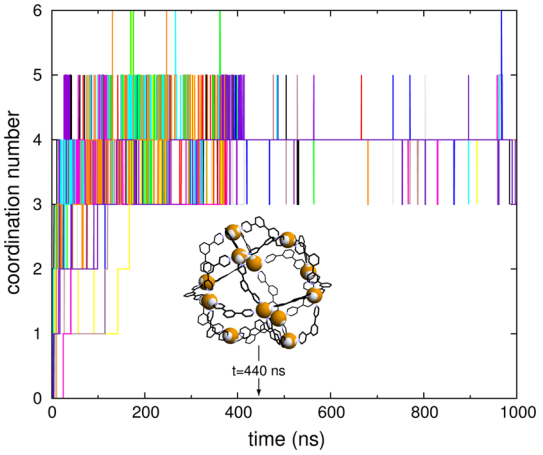

Figure 4. Time variations of the coordination numbers of the 12 Pd(II) within the completed $M_{12}L_{24}^{a}$ nanocage. Snapshots at the simulation time of 440 ns are additionally shown in the figure.

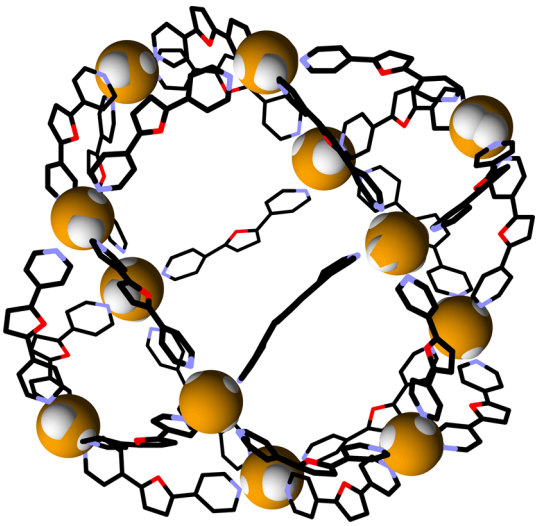

Figure 6. $M_{12}L_{24}^{b}$ nanocage from the snapshot after the 500 ns LD run.

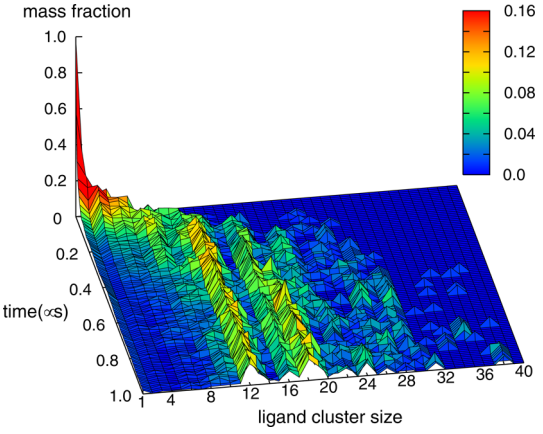

Figure 7. Cluster size distributions of the ligand a as a function of time. The vertical axis corresponds to the mass fractions.

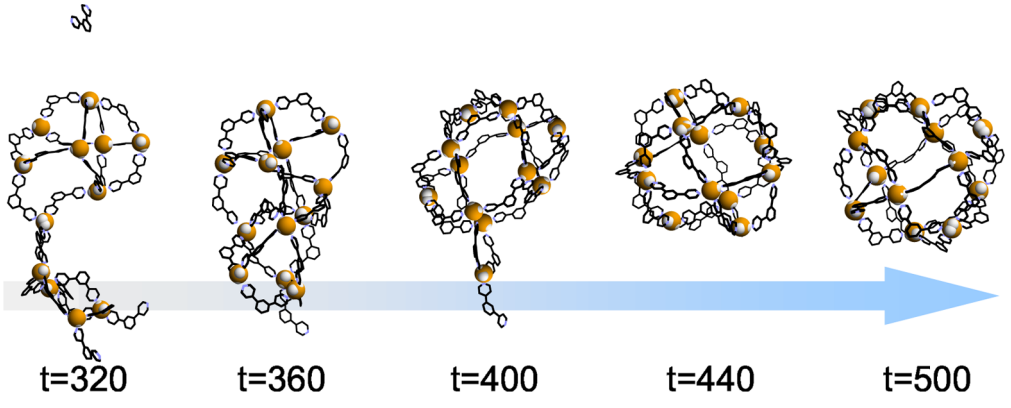

Figure 5. Structure change during the evolution stage in Figure 4.

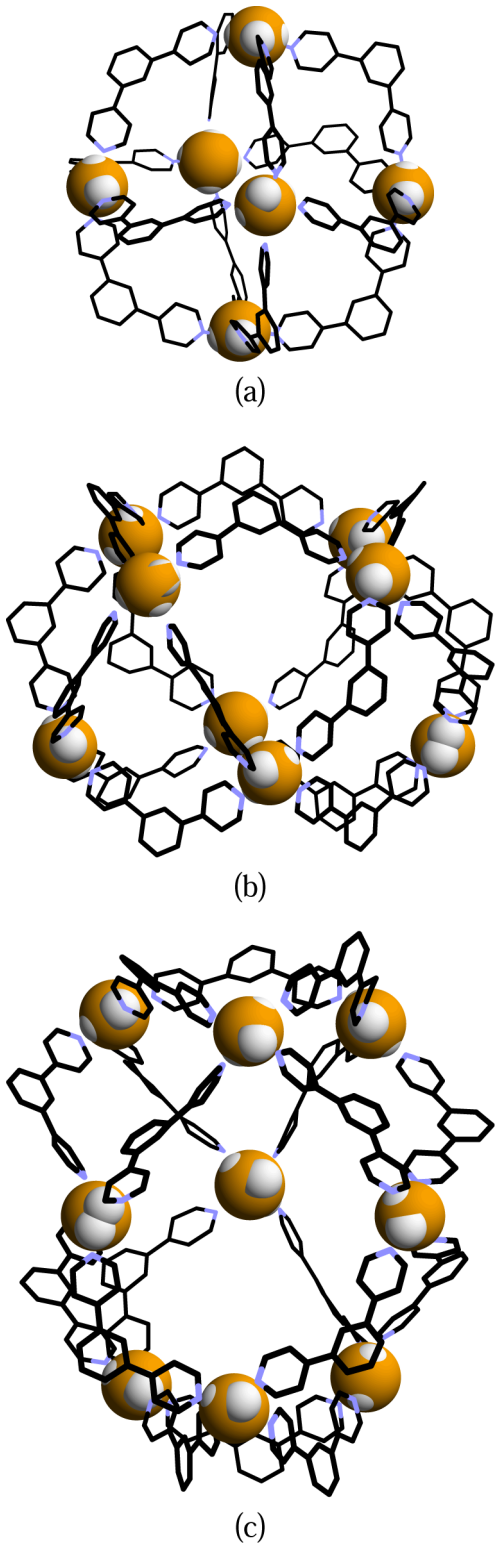

Figure 8. (a) $M_6L^a_{12}$, (b) $M_8L^a_{16}$ and (c) $M_9L^a_{18}$ cages from the snapshot after 1 μs LD run shown in the Figure 7.

mass fractions. Here, a ligand cluster size of 24 corresponds to the completed $M_{12}L^a_{24}$. As shown in this figure, the mass fraction for 24-sized clusters at the final step (1.0 μs) was *ca.* 0.1, which corresponds to 3−4 $M_{12}L^a_{24}$ cages assembly, compared with 1.0 for a

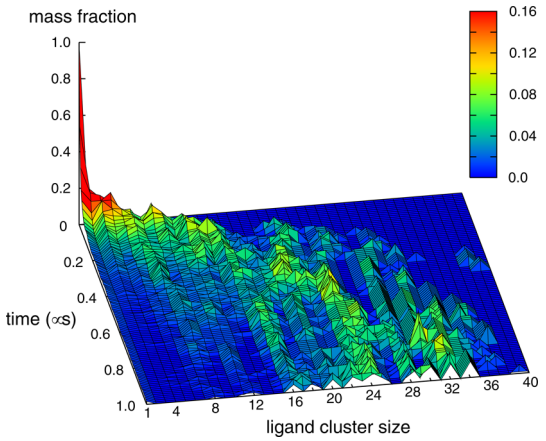

Figure 9. Cluster size distributions of the ligand b as a function of time. The vertical axis corresponds to the mass fractions.

100% yield assembly. In contrast, we observe peaks at 12, 16, and 18 for the larger fraction at approximately 0.14, 0.1, and 0.15 (corresponds to 4−9 nanocages), respectively. These smaller-sized clusters correspond to the lower-nuclearity complexes with specific symmetries. A peak for the ligand cluster size 12 corresponds to the cube shape $M_6L^a_{12}$ cage (shown in Figure 8a) whose formation was reported in a real reaction system of bidentate ligand with acetylene spacers (ligand **c** in Figure 1) with using platinum (Pt) instead of the Pd ion.[16] The latter peaks at 16 and 18 correspond to the $M_8L^a_{16}$ and $M_9L^a_{18}$ nanocages shown in Figure 8, panels b and c, respectively. These two cages are composed of eight three-ligand membered rings as in $M_{12}L^a_{24}$, but two and three (instead of six for the $M_{12}L^a_{24}$) four-ligand membered rings in the $M_8L^a_{16}$ and $M_9L^a_{18}$ nanocages, respectively. In these smaller nanocages ($M_6L^a_{12}$, $M_8L^a_{16}$ and $M_9L^a_{18}$), the coordination network geometries around the Pd(II) ions were deformed compared with $M_{12}L^a_{24}$. These geometry distortions were not so large as being toward tetrahedral geometry from the original coplanar one, but relatively small out-of-plane and adjacent angle deformations between the coordinated pyridines. The result above shows that the larger $M_{12}L_{24}$ self-assembly process noticeably involves the trapping structures with lower-nuclearity in contrast to the smaller M_6L_8 cage.

We also tried corresponding simulations with the furan-cored ligand **b**. Figure 9 shows the ligand cluster size distributions as a function of time which corresponds to the Figure 7 for the ligand **a**. The mass fraction for 24-sized clusters at the final step (around 0.1) is similar to that in Figure 7 for the ligand **a**. However, the peaks for the smaller-sized clusters (at 12, 16 and 18) were much suppressed compare to Figure 7. It is highly probable that the slightly larger bend angle (*ca.* 127°[22]) of the furan-cored ligand **b** would make those smaller-sized clusters energetically unfavorable compared to the ligand **a**. This shows the trapping at the

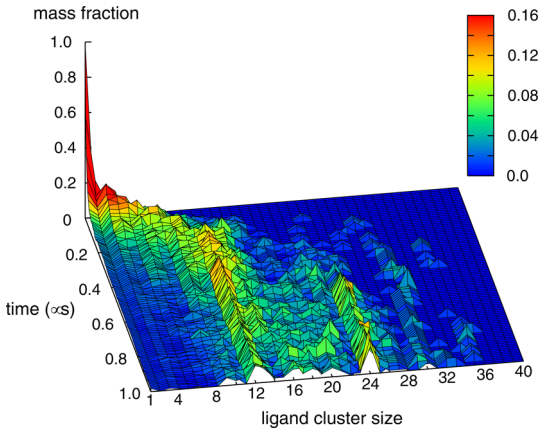

Figure 10. Cluster size distributions of the ligand a as a function of time with increasing of metal−ligand binding strength 2.0% after 300 ns in the run shown in Figure 7.

lower-nuclearities sensitively depends on the bend angle of ligands and slightly lager bend angle (compare to the geometrically optimum angle for the final structure, here 120° for $M_{12}L_{24}$[23]) would be effective to suppress the trapping.

As mentioned above, in the bidentate ligand real reaction system with using Pt(II) instead of the Pd(II) ion, the deformed $Pt(II)_6L^c_{12}$ cube, instead of $Pt(II)_{12}L^c_{24}$ sphere was observed.[16] It is proposed that the angle between the pyridyl coordination vectors (bend angle) determines which structure is observed experimentally.[2,23,24] Indeed, formation of M_6L_{12} cube using the ligands with a 90° bend angle[5] follows the proposed hypothesis. However, $Pt(II)_6L^c_{12}$ *vs* $Pd(II)_{12}L^c_{24}$ formation from the same ligand **c** (with the bend angle ~120°) is unpredicted from the hypothesis.[22] It is said that the stronger metal−ligand binding energy by the Pt(II) ion kinetically stabilizes the metastable complex $Pt(II)_6L^c_{12}$ even with the deformation energy penalties.[16]

Correspondingly, we tried a couple of simulations with changing the metal−ligand binding energy. Higher yield peak (*ca.* 0.18 mass fraction) at the ligand cluster size of 24 with suppressed yield peaks at 18 was obtained as shown in Figure 10 by increasing of metal−ligand binding strength 2.0% after 300 ns in the run shown in Figure 7. Here, 2.0% increase of the metal−ligand binding energy (pure Coulombic in the current model) was made by increasing negative atomic charge values (2.0%) on the ligand nitrogen while keeping the ligand charge neutrality. Results above show that the connection between the kinetic trapping and the binding strength and importance of the kinetic effects in the metal−ligand self-assembly.

We also realized that the pronounced changes between Figure 7 and Figure 10 do not occur if we applied the same binding strength increasing at the very beginning of the simulation, *i.e.*, the timing is important. The binding strength increased timing, 300 ns, roughly corresponds to the time of beginning of $M_{12}L_{24}$ cage formation in the simulation shown in Figure 7. We would like to discuss this point further in the following section, since it implies a hint to improve the current model.

As described in the Methods section, the atomic charges of our ligand models were assigned by the molecular orbital calculations (MO) of the ligands alone and we fixed those values in the course of MD simulations (*static* charge model). Upon complexation, there could be electronic rearrangement of metal ions and ligands, and then the total energy of the resultant complex is lowered. However, conventional MD simulations (including this study) were done with the potential energy functions based on the static charge model which does not take into account the electronic rearrangement upon complexation.[25] Recently, improved models aiming to better describe the electronic rearrangement in proteins containing metals have been proposed.[26] Sakharov and Lim proposed a *context-dependent* electrostatic model including charge transfer and local polarization effects.[27] They reported that these effects play an important role to reproduce the experimentally observed Zn(II)-ligand coordination structures. With MO calculations, we found that charge transfer and local polarization of Pd(II)−pyridine complex, which is simplified fragment of our current system are comparable with those in Zn(II)[27] and Cd(II) and Hg(II)[28] complexes (see the Supporting Information for details). This implies that application of the *context-dependent* electrostatic model to the Pd(II)-ligand system in this study would also be effective to improve the current model. We suppose that the increasing the negative atomic charges on the ligand nitrogen applied after 300 ns in the run shown in Figure 10 partly accounts for the *context-dependent* local polarization upon complexation.

CONCLUSIONS

The capabilities of our model originally developed for the self-assembly of the M_6L_8 system were examined by applying it to the larger $M_{12}L_{24}$ system. We are convinced that our model is capable of realizing self-assembly of this $M_{12}L_{24}$ in the distinct three-stage process for the two kinds of ligands. In contrast to the smaller M_6L_8 cage, we found that the larger $M_{12}L_{24}$ self-assembly process noticeably involves the kinetically trapped structures with the lower-nuclearities. We also found that the kinetic trapping behaviors sensitively depend on the bend angle of ligands and the metal−ligand binding strength. Our simulation result showed that slightly lager bend angle compared to the geometrically optimum angle for the final structure would be effective to suppress the trapping. Those kinetic effects become important factor when the number of the components becomes large as that of

$M_{12}L_{24}$ in this study. The results in this study imply that the kinetic effects would be one of the reason to make the prediction of self-assembled structures (*e.g.*, based on the bend angle of the ligands) increasingly difficult in the higher-nuclearity complexes.[22] We consider that the MD simulation could be valuable tool to study the kinetic effects in the metal−ligand coordination-directed self-assembly.

METHODS

We used the simulation model developed in our previous study[13] with the exception that the ligand molecule was replaced with the bidentate ligands in Figure 1. We applied a coarse-grained solvent model which combines the three methods, Langevin dynamics (LD),[29] the generalized reaction field method[30] and Weeks-Chandler-Andersen (WCA) type short-range repulsive potentials.[31] As in our previous study, we did not include the nitrate (NO_3^-) ions because they compete with the ligands for Pd(II) ions and, then, interfere with the nanocage self-assembly within the available computational time. [The results in our previous simulations on the M_6L_8 system (with and without the nitrate ions), imply that the M_6L_8 formations are highly probable to take place in the nitrate poor regions first compares to the nitrate rich regions. Then, our nitrate free model can be considered to model such the nitrate poor regions in the real system.]

For the metal−ligand coordination interaction, we applied the cationic dummy atom (CaDA) model[32] for Pd(II). The atomic charge of the Pd divalent cation evenly transferred to the four dummy atoms that were attached coplanarly to the Pd (the Pd−dummy distance was defined to reproduce the average Pd−N distance from the XRD study.[13]) For the bidentate ligands, we applied the flexible united-atom model [In our previous study on the M_6L_8 system, we used the nonstandard high barriers for some torsional potentials to maintain the tripodal nonplanar shape of the triandete ligand model. In contrast, we used standard force field parameters entirely for the bidentate ligands in the current study.] with the exception that the bond-stretching degrees of freedom were constrained to the equilibrium bond lengths. For the intermolecular and intramolecular interactions, a general AMBER force field[33] was used in combination with CH and CH_2 united atom parameters from a reoptimized united atom force field.[34] For Pd atoms, we used parameters from the literature.[35] For the ligand atomic charges, we used restrained electrostatic potential (RESP) charges,[36] obtained using *ab initio* molecular orbital calculations with the B3LYP/6-31G(d) level in the Gaussian03 program.[37]

Trajectories were produced using the MD program GROMACS (version 4.0.7)[38] with a modified nonbonded interaction routine to employ the WCA potential described above. For LD time integration, we used the leapfrog stochastic dynamics integrator[39] and LINCS bond constraint[40] with a 5 fs time step due to the stability of the LINCS algorithm.[41] Charge group-based, twin-range 0.65 nm van der Waals and 1.4 nm electrostatic cutoff distances[42] were applied to the nonbonded interactions. The setting of the former short value (0.65 nm) is because of the utilization of the short-ranged WCA potential. The far-field relative dielectric constant in the generalized reaction field method, ε_{rf}, was 47.0 for the DMSO solvent setting.[43] The near-field dielectric constants, ε_r, was 2.5 because this value was the optimum value found in our previous study. The simulation temperature was maintained by coupling to a stochastic thermostat with the time constant $\tau_t = 0.1$ ps *via* LD. The LD friction coefficient for each atom was specified as the GROMACS default value (*i.e.*, mass/τ_t).

The GROMACS molecular topology file for the ligand **a** and CaDA Pd(II) models with the atomic charge assignments that aided in reproducing the simulation in this study are presented in the Supporting Information. The topology file for the ligands was created using the program "acpype"[44] as the interface for the automatic atom type and bond type perception program "antechamber",[45] and then the output topology file was modified for the united atoms.

Conflict of Interest: The authors declare no competing financial interest.

Acknowledgment. We would like to thank Prof. D. C. Rapaport of Bar-Ilan University for his valuable discussions. This work was partly supported by KAKENHI (Grant-in-Aid for Scientific Research) in the Priority Area "Emergence in Chemistry" from the Ministry of Education, Culture, Sports, Science and Technology of Japan.

Supporting Information Available: Details of the molecular orbital calculations of the Pd(II)−pyridine complex. The GROMACS molecular topology file for the ligand **a** and CaDA Pd(II) models with the atomic charge assignments. This material is available free of charge *via* the Internet at http://pubs.acs.org.

REFERENCES AND NOTES

1. Lehn, J. *Supramolecular Chemistry*: Concepts and Perspectives; VCH: Weinheim, Germany, 1995.
2. Cook, T. R.; Zheng, Y.-R.; Stang, P. J. Metal−Organic Frameworks and Self-Assembled Supramolecular Coordination Complexes: Comparing and Contrasting the Design, Synthesis, and Functionality of Metal−Organic Materials. *Chem. Rev.* **2012**, *113*, 734–777.
3. McMorran, D. A.; Steel, P. J. The First Coordinatively Saturated, Quadruply Stranded Helicate and Its Encapsulation of a Hexafluorophosphate Anion. *Angew. Chem., Int. Ed. Engl.* **1998**, *37*, 3295–3297.
4. Liao, P.; Langloss, B. W.; Johnson, A. M.; Knudsen, E. R.; Tham, F. S.; Julian, R. R.; Hooley, R. J. Two-Component Control of Guest Binding in a Self-Assembled Cage Molecule. *Chem. Commun.* **2010**, *46*, 4932–4934.
5. Suzuki, K.; Tominaga, M.; Kawano, M.; Fujita, M. Self-Assembly of an M_6L_{12} Coordination Cube. *Chem. Commun.* **2009**, 1638–1640.
6. Moulton, B.; Lu, J.; Mondal, A.; Zaworotko, M. J. Nanoballs: Nanoscale Faceted Polyhedra with Large Windows and Cavities. *Chem. Commun.* **2001**, 863–864.
7. Eddaoudi, M.; Kim, J.; Wachter, J.; Chae, H.; O'keeffe, M.; Yaghi, O. Porous Metal-Organic Polyhedra: 25 Å Cuboctahedron Constructed from 12 Cu_2 (CO_2) 4 Paddle-Wheel Building Blocks. *J. Am. Chem. Soc.* **2001**, *123*, 4368–4369.
8. Tominaga, M.; Suzuki, K.; Kawano, M.; Kusukawa, T.; Ozeki, T.; Sakamoto, S.; Yamaguchi, K.; Fujita, M. Finite, Spherical Coordination Networks that Self-Organize from 36 Small Components. *Angew. Chem., Int. Ed.* **2004**, *43*, 5621–5625.
9. Sun, Q.; Iwasa, J.; Ogawa, D.; Ishido, Y.; Sato, S.; Ozeki, T.; Sei, Y.; Yamaguchi, K.; Fujita, M. Self-Assembled $M_{24}L_{48}$ Polyhedra and Their Sharp Structural Switch upon Subtle Ligand Variation. *Science* **2010**, *328*, 1144.
10. Li, Z.; Kishi, N.; Hasegawa, K.; Akita, M.; Yoshizawa, M. Highly Fluorescent M_2L_4 Molecular Capsules with Anthracene Shells. *Chem. Commun.* **2011**, *47*, 8605–8607.
11. Han, M.; Michel, R.; He, B.; Chen, Y.-S.; Stalke, D.; John, M.; Clever, G. H. Light-Triggered Guest Uptake and Release by a Photochromic Coordination Cage. *Angew. Chem., Int. Ed.* **2013**, *52*, 1319–1323.
12. Harris, K.; Fujita, D.; Fujita, M. Giant Hollow M_nL_{2n} Spherical Complexes: Structure, Functionalisation and Applications. *Chem. Commun.* **2013**, *49*, 6703–6712.
13. Yoneya, M.; Yamaguchi, T.; Sato, S.; Fujita, M. Simulation of Metal−Ligand Self-Assembly into Spherical Complex M_6L_8. *J. Am. Chem. Soc.* **2012**, *134*, 14401–14407.

14. Chand, D.; Biradha, K.; Fujita, M.; Sakamoto, S.; Yamaguchi, K. A Molecular Sphere of Octahedral Symmetry. *Chem. Commun.* **2002**, 2486–2487.
15. Palma, C.-A.; Cecchini, M.; Samor, P. Predicting Self-Assembly: from Empirism to Determinism. *Chem. Soc. Rev.* **2012**, *41*, 3713–3730.
16. Fujita, D.; Takahashi, A.; Sato, S.; Fujita, M. Self-Assembly of Pt (II) Spherical Complexes *via* Temporary Labilization of the Metal−Ligand Association in 2,2,2-Trifluoroethanol. *J. Am. Chem. Soc.* **2011**, *133*, 13317–13319.
17. Sato, S.; Iida, J.; Suzuki, K.; Kawano, M.; Ozeki, T.; Fujita, M. Fluorous Nanodroplets Structurally Confined in an Organopalladium Sphere. *Science* **2006**, *313*, 1273.
18. Murase, T.; Sato, S.; Fujita, M. Nanometer-Sized Shell Molecules That Confine Endohedral Polymerizing Units. *Angew. Chem., Int. Ed.* **2007**, *46*, 1083–1085.
19. Fujita, D.; Suzuki, K.; Sato, S.; Yagi-Utsumi, M.; Yamaguchi, Y.; Mizuno, N.; Kumasaka, T.; Takata, M.; Noda, M.; Uchiyama, S.; *et al.* Protein Encapsulation within Synthetic Molecular Hosts. *Nat. Commun.* **2012**, *3*, 1093.
20. Scheraga, H. A.; Khalili, M.; Liwo, A. Protein-Folding Dynamics: Overview of Molecular Simulation Techniques. *Annu. Rev. Phys. Chem.* **2007**, *58*, 57–83.
21. Sato, S.; Ishido, Y.; Fujita, M. Remarkable Stabilization of $M_{12}L_{24}$ Spherical Frameworks through the Cooperation of 48 Pd (II)- Pyridine Interactions. *J. Am. Chem. Soc.* **2009**, *131*, 6064–6065.
22. Bunzen, J.; Iwasa, J.; Bonakdarzadeh, P.; Numata, E.; Rissanen, K.; Sato, S.; Fujita, M. Self-Assembly of $M_{24}L_{48}$ Polyhedra Based on Empirical Prediction. *Angew. Chem., Int. Ed.* **2012**, *51*, 3161–3163.
23. Williams, A. F. Ligand Design for Hollow Spherical Complexes. *Coord. Chem. Rev.* **2011**, *255*, 2104–2110.
24. Leininger, S.; Olenyuk, B.; Stang, P. J. Self-Assembly of Discrete Cyclic Nanostructures Mediated by Transition Metals. *Chem. Rev.* **2000**, *100*, 853–908.
25. Sousa, S.; Fernandes, P.; Ramos, M. Molecular Dynamics Simulations: Difficulties, Solutions and Strategies for Treating Metalloenzymes. *Kinet. Dyn.* **2010**, 299–330.
26. Peraro, M. D.; Spiegel, K.; Lamoureux, G.; Vivo, M. D.; DeGrado, W. F.; Klein, M. L. Modeling the Charge Distribution at Metal Sites in Proteins for Molecular Dynamics Simulations. *J. Struct. Biol.* **2007**, *157*, 444–453.
27. Sakharov, D. V.; Lim, C. Zn Protein Simulations Including Charge Transfer and Local Polarization Effects. *J. Am. Chem. Soc.* **2005**, *127*, 4921–4929.
28. Sakharov, D. V.; Lim, C. Force Fields Including Charge Transfer and Local Polarization Effects: Application to Proteins Containing Multi/Heavy Metal Ions. *J. Comput. Chem.* **2009**, *30*, 191–202.
29. Yun-yu, S.; Lu, W.; Van Gunsteren, W. On the Approximation of Solvent Effects on the Conformation and Dynamics of Cyclosporin A by Stochastic Dynamics Simulation Techniques. *Mol. Simul.* **1988**, *1*, 369–383.
30. Tironi, I.; Sperb, R.; Smith, P.; van Gunsteren, W. A Generalized Reaction Field Method for Molecular Dynamics Simulations. *J. Chem. Phys.* **1995**, *102*, 5451.
31. Weeks, J.; Chandler, D.; Andersen, H. Role of Repulsive Forces in Determining the Equilibrium Structure of Simple Liquids. *J. Chem. Phys.* **1971**, *54*, 5237.
32. Pang, Y. Novel Zinc Protein Molecular Dynamics Simulations: Steps Toward Antiangiogenesis for Cancer Treatment. *J. Mol. Model.* **1999**, *5*, 196–202.
33. Wang, J.; Wolf, R. M.; Caldwell, J. W.; Kollman, P. A.; Case, D. A. Development and Testing of a General Amber Force Field. *J. Comput. Chem.* **2004**, *25*, 1157.
34. Tiberio, G.; Muccioli, L.; Berardi, R.; Zannoni, C. Towards *in Silico* Liquid Crystals. Realistic Transition Temperatures and Physical Properties for n-Cyanobiphenyls *via* Molecular Dynamics Simulations. *ChemPhysChem* **2008**, *10*, 125.
35. Calligaris, M.; Zangrando, E.; Milani, B.; Marson, A. Stereochemical Investigation of Palladium (II) Complexes with Phenanthroline Ligands: A Molecular Mechanics Approach. *Eur. J. Inorg. Chem.* **2005**, *2005*, 704–712.
36. Bayly, C. I.; Cieplak, P.; Cornell, W.; Kollman, P. A. A Well-Behaved Electrostatic Potential Based Method Using Charge Restraints for Deriving Atomic Charges: the RESP Model. *J. Chem. Phys.* **1993**, *97*, 10269.
37. Frisch, M. J.; Trucks, G. W.; Schlegel, H. B.; Scuseria, G. E.; Robb, M. A.; Cheeseman, J. R.; Montgomery, J. J. A.; Vreven, T.; Kudin, K. N.; Burant, J. C. *et al. Gaussian03*, Revision C.02; Gaussian, Inc.: Wallingford, CT, 2004.
38. Hess, B.; Kutzner, C.; Van Der Spoel, D.; Lindahl, E. GROMACS 4: Algorithms for Highly Efficient, Load-Balanced, and Scalable Molecular Simulation. *J. Chem. Theory Comput.* **2008**, *4*, 435–447.
39. van Gunsteren, W.; Berendsen, H. A Leap-Frog Algorithm for Stochastic Dynamics. *Mol. Simul.* **1988**, *1*, 173–185.
40. Hess, B.; Bekker, H.; Berendsen, H. J. C.; Fraaije, J. G. E. M. LINCS: A Linear Constraint Solver for Molecular Simulations. *J. Comput. Chem.* **1997**, *18*, 1463.
41. Feenstra, K. A.; Hess, B.; Berendsen, H. J. Improving Effciency of Large Timescale Molecular Dynamics Simulations of Hydrogen-Rich Systems. *J. Comput. Chem.* **1999**, *20*, 786–798.
42. Lindahl, E.; Hess, B.; van der Spoel, D. GROMACS 3.0: A Package for Molecular Simulation and Trajectory Analysis. *J. Mol. Model.* **2001**, *7*, 306.
43. Villa, A.; Mark, A.; Saracino, G.; Cosentino, U.; Pitea, D.; Moro, G.; Salmona, M. Conformational Polymorphism of the PrP106−126 Peptide in Different Environments: A Molecular Dynamics Study. *J. Phys. Chem. B* **2006**, *110*, 1423–1428.
44. da Silva, A. W. S.; Vranken, W. F. ACPYPE-AnteChamber PYthon Parser interfacE. *BMC Res.Notes* **2012**, *5*, 367.
45. Wang, J.; Wang, W.; Kollman, P.; Case, D. Automatic Atom Type and Bond Type Perception in Molecular Mechanical Calculations. *J. Mol. Graphics Modell.* **2006**, *25*, 247–260.